ANALYSIS OF DEFECTS AND FAULT MODELS IN EMBEDDED SPIN TRANSFER TORQUE (STT) MRAM ARRAYS

A Thesis
Presented to
The Academic Faculty

by

Ashwin Chintaluri

In Partial Fulfillment
of the Requirements for the
Masters Degree in the
School of Electrical and Computer Engineering

Georgia Institute of Technology
May 2016

ANALYSIS OF DEFECTS AND FAULT MODELS IN EMBEDDED SPIN TRANSFER TORQUE (STT) MRAM ARRAYS

Approved by:

Dr. Arijit Raychowdhury, Advisor
School of Electrical and Computer Engineering
Georgia Institute of Technology

Dr. Saibal Mukhopadhyay
School of Electrical and Computer Engineering
Georgia Institute of Technology

Dr. Moinuddin K. Qureshi
School of Electrical and Computer Engineering
Georgia Institute of Technology

Date Approved: 4/26/2016

Dedicated to my parents.

ACKNOWLEDGEMENTS

First and foremost, I would like to express my deep sense of gratitude to my advisor, Professor Arijit Raychowdhury for his insightful guidance throughout my research work. His vast knowledge of the subject and his ability to formulate innovative solutions to problems has helped me greatly in working towards this thesis.

I would like to thank Dr. Suriyaprakash Natarajan (Intel) and Dr. Helia Naemi (Intel) for their collaboration and for their valuable inputs throughout the project.

I am very grateful to Professor Saibal Mukhopadhyay and Professor Moinuddin Qureshi for agreeing to be on my thesis committee.

I am thankful to all the past and present members of Integrated Circuits& Systems Research Lab notably Abhinav Parihar, Anvesh Amaravati, Insik Yoon, Samantak Gangopadhyay, Soham Desai, Saad Nasir and Ashwin Subramanian for their support and valuable discussions which helped in my thesis.

Finally, I would like to thank my parents and family without whose continuous support I would not have been able to achieve any of this.

TABLE OF CONTENTS

LIST OF TABLES

LIST OF FIGURES

SUMMARY

Spin transfer torque magnetic random access memory (STT-MRAM) is a competitive, future memory technology that has gained immense interest in recent years due to its small cell size, voltage and process compatibility with CMOS and nano-second read/write speeds. It exhibits high density (3-4x of SRAM), non-volatility and process scalability and hence is widely being considered as a viable alternative for SRAM in last-level caches. As the design and fabrication process matures for the STT-MRAM, there is a need to study the various fault models that can affect this novel memory technology. This work presents a comprehensive analysis of fault models in STT-MRAM under both parametric variations as well as resistive defects (opens and shorts). Sensitivity of read, write and retention to process parameter variations such as lithographic and material variations are studied. In addition, defects (both intra-cell and inter-cell) and the corresponding fault models have been studied and data patterns which excite these faults are explored.

CHAPTER 1

I. INTRODUCTION

With an ever-increasing demand for larger on-die memory while traditional CMOS scaling hitting the atomic scale boundaries [1], there is an urgent need to explore novel memory technologies. Many hybrid CMOS memory technologies like STT-MRAM, R-RAM, PCM, are being considered by the research community and industry today as alternatives to the traditional SRAM based on-die memory. These memories use nanoscaled devices with unique material properties that change state under the influence of electric or magnetic fields. These state changes are leveraged for bit level storage. Since such state changes are preserved even after removing the stimulus and supply, these CMOS hybrid technologies are perceived to have high levels of non-volatility. Among these, Spin Torque Transfer (STT)-MRAM is considered a promising candidate, as an alternative to embedded DRAM (eDRAM) and SRAM due to its high density, non-volatility, high endurance, easy integration with the existing CMOS fabrication process and nanosecond access times[1,2,3]. It has emerged as a successor to MRAM by providing current induced write in scaled process nodes [1]. The huge potential of STT-MRAM as a viable embedded memory technology at advanced process nodes has been well demonstrated in the 45nm [4] and 65nm [5] technology nodes. As the STT-MRAM technology continues to mature, rigorous analysis of variability and failure in this novel resistive memory need to be studied in detail. Previous research [6,7,8,9,10] has reported the effects of parametric variations in the read and write access times and failure probabilities in STT-MRAM. On the other hand, the effects of injected defects and the corresponding failure models in STT-RAM have not been extensively studied in the past research. [11,12,13] have studies the defects and fault models of SRAM. More recently, research [14,15,16,17,18] has addressed fault modelling in Memristor arrays by injecting electrical defects and identified possible faults in Memristor arrays. But, because of the fundamental differences in operation between

SRAM, Memristor and STT-MRAM, not all fault types discussed in previous research is applicable to STT-MRAM. As an example, STT-MRAM, being a truly bi-stable device, does not suffer from the dynamic Write disturb Fault (dWdF) identified in [17]. Also, [14,17] mostly identify static fault models due to the injected electrical faults. However, there are also many dynamic faults that are possible due to simultaneous switching of two cells together in presence of bridge defects. In addition, STT-MRAM faces its own unique set of possibilities of failure and faults due to parametric variations and injected defects, which we explore in this work.

In this work, we aim to provide a comprehensive treatment and classification of the fault models manifesting due to both parametric variations and electrical faults in STT-MRAM memory arrays. We consider the three main modes of failure – Read failure, Write failure and Retention failure that are prevalent in STT-MRAM and analyze the fault models that lead to these failures.

- We study sensitivity of Write (WR) and Read (RD) with the parameter variations and identify the fault models that manifest due to variations. Failure probability of Write, Read and Retention are studied.
- We inject electrical faults at an array level and formulate the fault primitives occurring in the cell. We discuss about the Data-dependent Coupling Faults that we discovered. Further, we identify the data patterns that sensitize each of the documented faults leading to failure.
- We consider the interplay of parameter variations and the electrical faults and the effect on failure.

CHAPTER 2

BACKGROUND

2.1 THE BASIC 1T-1R STT-MRAM CELL

When a spin-polarized current passes through a mono-domain ferromagnet, it attempts to polarize the current in its preferred direction of magnetic moment. As the ferromagnet absorbs some of the angular momentum of the electrons, it creates a torque that causes a flip in the direction of magnetization in the ferromagnet. The basic STT-MRAM cell

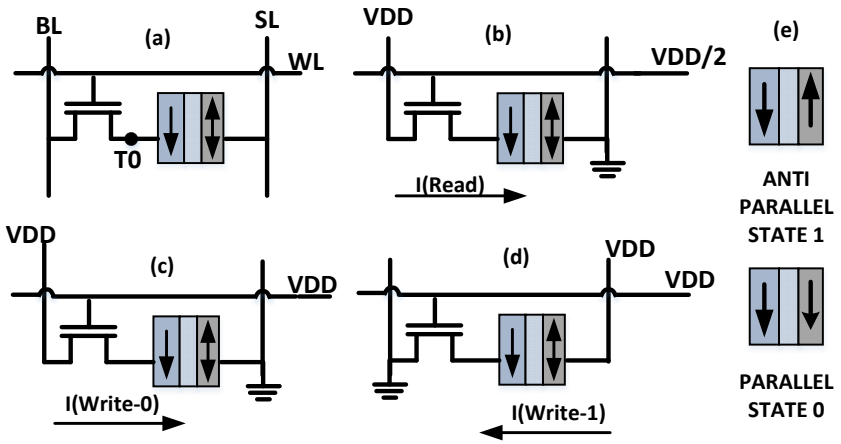

Figure. 1: Basic STT-MRAM cell (a) 1T-1MTJ representation (b) bias condition for read (c) write 0 bias condition (d) write 1 bias condition (e) States in a MTJ due to orientation of magnetic moments.

comprises of an access transistor and a Magnetic Tunneling Junction (MTJ) as shown in Figure 1(a). The MTJ, which is the storage element in the cell, consists of a tunneling oxide (MgO) sandwiched between two ferromagnetic layers (CoFeB based), one of which has a fixed magnetization and the other is a free layer. The fixed layer is the polarizer (reference) and the free layer acts as the storage node. The relative alignment of the ferromagnetic layers results in a high resistance path (anti-parallel) or a low resistance (parallel) path for the current, giving a notion of binary storage. Depending on the direction of current of a sufficient density, the free layer magnetization flips from Anti-parallel to Parallel state or

vice versa resulting in change of bit from 1 to 0 or 0 to 1 respectively. Figure 1 (b) – (d) illustrates the bias conditions applied for the read and write operations. For our study, we consider that the fixed layer is connected to the access transistor. As one can see, the write operation is bidirectional, where either the bit-line (BL) or source line (SL) is pulled high and the other one is pulled low depending on the polarity of the write operation. The read operation is unidirectional with an under-driven word line voltage (WL), where a pre-charged BL voltage is allowed to discharge through the cell, the rate of discharge being governed by the resistive state of the cell.

For an STT-MRAM cell to qualify as a non-volatile memory cell, it should satisfy the fundamental properties of readability, writability and stability (retention) [19]. These three properties depend closely on the material, electrical and design parameters of both the MTJ as well as the access transistor. The key macroscopic parameters whose variations control the overall failure probabilities in STT-RAM arrays are:

1. **MTJ Material parameters:**
    i. The magnetic anisotropy (H_K),
    ii. Saturation magnetization (M_S),
    iii. Tunnel Magneto-resistance ratio(TMR),
    iv. Oxide thickness of MgO layer (T_{OX}).
2. **Transistor Electrical parameters:**
    i. Threshold voltage V_{TH} of the access transistor.
3. **Design Parameters (Lithographic):**
    i. Planar dimensions of the MTJ and Length and Width variations of the access transistor.

In addition, the thermal stability factor for an STT-MRAM, which is defined by a measure of the stored internal energy, is estimated as $\Delta \sim 1/2 M_S H_K V$, where V is the total volume of

the free layer nanomagnet. Authors in [2,6,8,20,21] explore the design space for some of these parameters with an emphasis on scalability.

2.2 The Macrospin Assumption

To understand the role of the design and material parameters in the process of read and write, a complete solution of the magnetic dynamics under a spin transfer torque current needs to be analyzed. This is typically done using a macrospin approximation of the free layer nanomagnet, as has been proposed in [22]. A macrospin model ignores interactions within the nanomagnet. A solution of the linearized Landau-Lifshitz-Gilbert (LLG) equation with the spin torque current demonstrates the close interaction of the device magnetics and the injected current. The linearized LLG equation is numerically solved to understand the switching dynamics of the free-layer magnetic-moment ***m(t)*** (figure 2) in presence of the torque experienced because of uniaxial anisotropy field ($\mathbf{T_U}$), easy plane anisotropy field ($\mathbf{T_K}$), and spin transfer torque from injected electrons ($\mathbf{T_S}$). The LLG under the total torque (**T**) is expressed as:

$$\frac{d\boldsymbol{m}(t)}{dt} + \alpha\left(\boldsymbol{m}(t)\ X\ \frac{d\boldsymbol{m}(t)}{dt}\right) = \gamma \boldsymbol{T} \qquad (1)$$

where α is the LLG damping coefficient γ is the gyromagnetic ratio. The solution of (1) is carried out in polar coordinates, and the transformed equation is:

$$\frac{1+\alpha^2}{\gamma H_K}\begin{bmatrix}\frac{d\theta}{dt}\\ \frac{d\phi}{dt}\end{bmatrix} = \boldsymbol{T_U} + \boldsymbol{T_K} + \boldsymbol{T_S} \qquad (2)$$

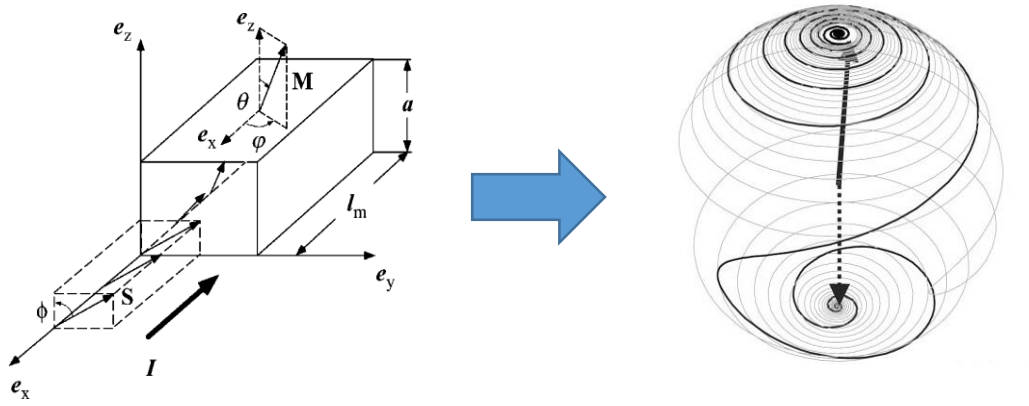

Figure 2 Macrospin Assumption of nanomagnet [22] (a) A macrospin nanomagnet with magnetic moment vector **M** (b) the precessional moment of the magnetic moment in a 3D representation.

where the free layer nanomagnet is in the $\phi=\pi/2$ plane. In a manner described in [17], the switching current density (J_{C0}) at T=0K can be described by:

where e is the electronic charge, η is the polarization of the injected current, and t is the thickness of the free layer. At non-zero temperatures, the thermal activation factor assists in switching and is included using a stochastic thermal model as described in [6]. More details of the model and its integration in the array level simulator is described in chapter 3. Equations (1) to (3) describe the process of write in STT-MRAM. The process of read is based on an electrical read-out of the difference in resistance between the parallel and anti-parallel configurations of the MTJ stack. A key material and design parameter, the Tunnel Magneto-resistance Ratio (TMR) is the ratio of difference between the high resistance, R_H (anti-parallel state) and low resistance R_L (parallel state) to the resistance R_L and is given by:

$$TMR = \left(\frac{R_H - R_L}{R_L}\right).100\% \qquad (4)$$

The MTJ can either be an In-plane MTJ (I-MTJ) with magnetic anisotropy in plane due to shape anisotropy or a Perpendicular plane MTJ (P-MTJ) where magnetic anisotropy is aligned out of plane independent of shape of free layer [1]. Typically, the MTJ is etched into the process in Back End of the Line (BEOL) after which the metal layers are laid out and this is required to be done at ~350C. Until quite recently, only I-MTJ process was mature enough to give good yield and therefore, initial STT MRAM prototypes were I-MTJ [1]. But with advancement of material and fabrication techniques, there have been demonstrations of successful P-MTJ based arrays in recent research. Authors in [24] taped out 8Mb 1T1MTJ STT-MRAM array using P-MTJ in 90nm process with cell size of $50F^2$, with read time of 4ns and write time of 4.5ns. [25] presents a 1Mb 1T1MTJ STT-MRAM array using P-MTJ in 28nm process with a cell size of $37F^2$ with 2ns write pulse and

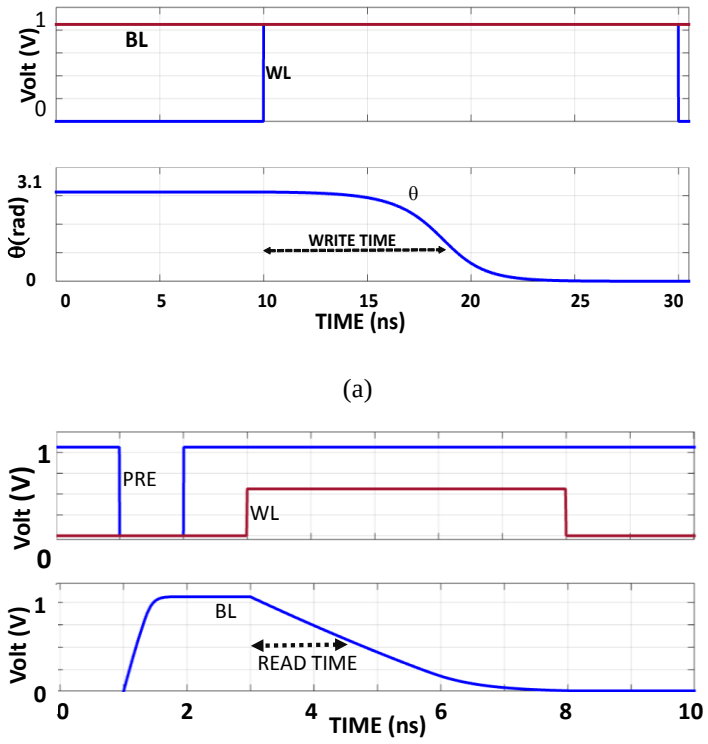

Figure 3: Basic operations in an MTJ based STT-RAM bit-cell (a) Write Operation, and (b) Read Operation.

50.7uA write current. P-MTJs are potential candidate for high density embedded memory due to high thermal stability and low critical current. In general, P-MTJ spin valves were manufactured with CoFeB free-layer/MgO tunneling barrier/CoFeB pinned layer with a [Co/Pd]n-SyAF (synthetic anti-ferro-magnetic layer. But the TMR achievable is not high enough (<100%) due to material properties and process conditions. [26] has shown that using a combination of Ta/CoFeB/MgO/CoFeB/Ta , TMR of >120% can be achieved. It has also been suggested that usage of double MgO layer in a P-MTJ can give good thermal stability $\Delta = KuV/kbT$, ~60 to get a 10 year retention [27]. Toshiba has reported an MTJ last process in [25] where the integration of MTJ is done as a final step and therefore need not undergo high temperatures thus eliminating the problem of TMR degradation. A high TMR assists in a stable, error free read even under process induced variations.

For our analysis, we have assumed the MTJ to be an In-plane MTJ that is currently known to give reasonable yields in manufacturing. In the following chapters, we explore the effects of defects and process induced variations on the process of read, write and retention.

CHAPTER 3

MODEL & SIMULATION INFRASTRUCTURE DEVELOPMENT

3.1 HSPICE model development

In the simplest form of static model proposed, STT MRAM can be modelled as a 1 transistor, 1 resistor model in which the resistance changes instantly between a high state and a low state when the correct bias is applied. But such a static model doesn't capture the continuously varying resistance and the current through the device. Our simulation model is based on the macrospin assumption of the free-layer nanomagnet [6,22] as described in Chapter 2. In our current study, an HSPICE based model for STT-MRAM has been developed using controlled current and voltage sources that emulate the spin dynamics. Details of the model development have been extensively reported in [6,10,23]. Interested readers are pointed to [23] for numerical techniques to solve LLG with spin transfer torque and to [10] for details on HSPICE compatible STT-MRAM models. The resistance of the MTJ stack, as the magnet undergoes precession from θ=0 to θ=π to is given by:

$$R(\theta,V,T) = \frac{\sin(cT)}{cT}[P_3\theta^3 + P_2\theta^2 + P_1\theta + R_L] \\ (1 - abs(V)/Slope).10^{s(Tox-Tox,0)} \quad (5)$$

where, V is applied voltage , c is a material constant, $P_{1\text{-}3}$ are fitting parameters and *Slope* determines voltage dependence of $R_{H.}$ This also captures the temperature dependence of resistance with the operating temperature (T). The MTJ model is fully parameterized using device and material parameters discussed in the next chapter, which allows comprehensive variation analysis. Variation analysis is done through extensive Monte Carlo simulations where both device-to-device and temporal variations are accounted for. This device model is incorporated in a bit-cell with a 2-fin FinFET selector transistor from a 14nm process node [29] and the design has been scaled up to an array with peripherals similar to conventional memory systems in a manner similar to the organization presented in [14]. This model features advanced simulation capabilities including: (a) simultaneous WR on different BL, (b) back-to-back RD/WR, (figure 3) (c) evaluation of sneak current paths through inter-cell bridges (d) and smart Monte-Carlo techniques with in-built response surface analysis for statistical data collection [6]. As an example, figure 3(a) illustrates the Write operation where the angle θ changes from π to 0 (anti-parallel to parallel). Figure 3(b) shows the read operation from a bit-cell in the array and demonstrates an underdriven WL that reduces the probability of any inadvertant write during read (read disturb). The nominal design parameters have been summarized in Table 1. We use the developed end-

TABLE 1: Nominal Design and Material Parameters

	Parameter	Nominal Values
Transistor	Length	14nm
	W_access	42nm
	Fins	2
	Vth	0.25V
MTJ	Width	40nm
	Length	100nm
	Tox	1.1nm
	Ms	800 emu/cc
	RA	10
	TMR	150%
	Hk	150 Oe

to-end simulation environment to study key material, device and circuit parameters and their roles in different failure mechanisms in the array.

Components in the HSPICE model are depicted in figure 4 and are as follows:

a) LLG component:

The LLG component models the switching dynamics of the free layer thereby giving information on the relative angle of magnetization with respect to the fixed layer. The linearized LLG equation is modelled using electrical elements based on Kirchhoff's law. Voltage dependent current sources are used to express the magnitude and direction of torques (figure 4(b)).The capacitance captures the dynamics of (Θ,φ). Initial voltages on the capacitors are used to specify initial position of magnetization.The resistances $R_{sx,y,z}$ correspond to the spin torque, $R_{fx,y,z}$ correspond to the thermal variations, $R_{hx,y,z}$ correspond to external magnetic field.

b) Transport component: The transport component emulates the time dependent MTJ resistance based on θ, φ estimated from the LLG component, the applied voltage, and temperature by (5)

The parameters $P_{3,2,1}$ are a function TMR ,*T*ox is the oxide thickness, R_P is the tunneling resistance in the parallel mode, *V* is the applied voltage, *c* is a material dependent parameter,

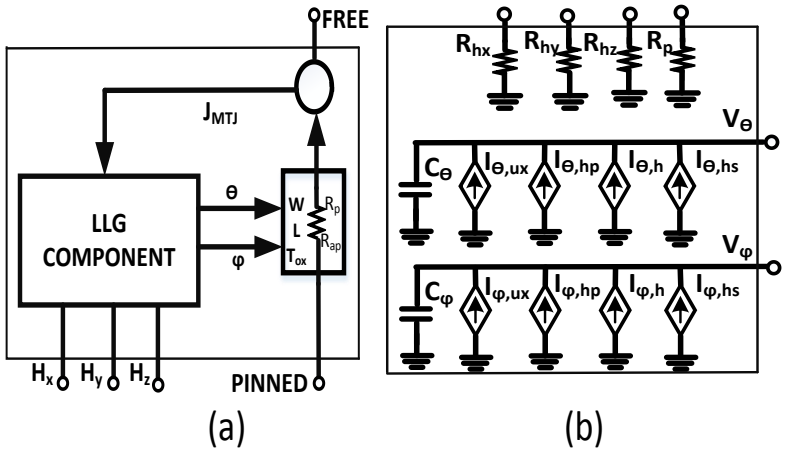

Figure 4: SPICE based MTJ model [10] (a) The MTJ subcircuit (b) The implementation of LLG equation.

and Slope determines the voltage dependence of *R*AP, T is the temperature. Thus the resistance is dependent on TMR and Tox of the MTJ which are inter related.

c) Thermal Component:

The write time of STT MRAM is highly dependent on temperature. Thermal variations are modelled as randomly varying current sources that feed to resistors in the $R_{fx,y,z}$ LLG component as thermal noise. This thermal variation is modelled as a noise on the angle of magnetization.

CHAPTER 4

PARAMETER VARIATON AND FAULT MODELS

Like every other memory technology, we expect STT-MRAM to also face process induced variations. The sources of variation in STT-MRAM bit-cells and arrays arise from process induced variations in both material and lithographic properties as well as noise generated by thermal effects. The major challenge of implementation of STT MRAM has been the design of bit cells under process variations. [6][8][9][20][21][28] discuss in details about various design tradeoffs that might be taken. [21] has shown that write performance will become the scaling bottleneck for P-MTJ. It has also been shown that beyond 22nm, in-plane MTJ is a feasible solution due to lower write current density than P-MTJ assuming a constant Jc0.RA/VDD scaling. This is due to the fact that critical current Ic0 scales as an exponential factor of alpha in an I-MTJ but is a constant in a P-MTJ. [22] has discussed several failure mitigation schemes for write, including WL boosting during write, BL or SL boosting, applying external magnetic field for write assist and adaptive body biasing of the transistor, and has shown that a combination of these schemes can reduce the width of access transistor.

In this chapter, we analyze the sensitivity of variations of parameters on the various operations on the STT-MRAM cell to understand what kind of control is needed on the design parameters. The main sources of parametric variations that we consider are summarized as:

MTJ Material Parameters: (a) normally distributed localized fluctuation of magnetic anisotropy, H_K [23], (b) Saturation Magnetization (M_S) (c) Tunnel Magneto-Resistance ratio (TMR) which is the ratio of difference between high and low resistances to the low resistance of MTJ, all with σ~10%.

Transistor Electrical Parameter: (a) normally distributed threshold voltage (V_t) with σ~10%.

Lithographic Variation: (a) normally distributed variation of planar dimensions with σ~10%, and (b) normally distributed variation of MgO thickness with (μ=1.1nm and σ=0.1nm).

Thermal Fluctuations: Thermal fields lead to variation in the magnetic dynamics by (a) changing the initial angle of precession and (b) adding a stochastic spin torque term in LLG which causes the write times to vary [22]. The dependence of read on temperature is captured through the dependence of the resistance on temperature (Eqn. (5)) and through read disturb, as will be discussed is Subsection 4.2. Retention failure is also largely dependent on the ambient temperature and is discussed in Subsection 4.3.

All these sources of variation lead to variations in RD, WR and Retention. Enough guard-bands are provided in designs for a target failure probability (P_{FAIL}), typically for a 6σ corner (P_{FAIL}~10^{-9}). Under extreme variations and defects, a particular bit-cell may fail (in RD, WR or retention) even when design margins up to 6σ guard-bands are used. Such a failure will manifest as a fault. Hence we need to: (a) understand how large the 6σ design guard-bands are, and (b) categorize the Fault Primitives and provide corresponding 'Fault Models'. Extreme parametric variations and/or defects during high-volume manufacturing can exceed RD, WR and Retention guard-bands, and are modeled as faults.

4.1. Write Operation & Failure

We first analyze the process of WR under parametric variation. A sensitivity of WR for a parameter, p is defined as S= $(\partial T_{WR}/T_{WR})/ (\partial p/p)$. The sensitivity analysis of WR time with respect to key process parameters shows large dependence on the transistor threshold voltage V_{TH} and the T_{OX} of the MTJ (figure 5(a)). This is followed by sensitivity on the saturation magnetization (M_S). The dependence on other parameters namely the Resistance-Area(RA) product[2] and the TMR are relatively less significant.

A 6σ cell is designed using the obtained write time spread from the variation analysis. For a target storage energy Δ_{TARGET}, it is observed that the 6σ values of T_{WRITE} are 3x-4x larger than the mean (figure 5(b)), which is significantly larger than competing memory technologies. Considering a nominal cell with T_{WRITE} =20ns for Δ_{TARGET} =60, if a 3.5x T_{WRITE} margin is provided for the worst-case cell, from figure 5(b) any cell with T_{WRITE}>60ns is deemed un-writable. We characterize this as a 0→1 or 1→0 **Transition Fault (TF1 or TF0),** where transition does not happen during the desired write window.

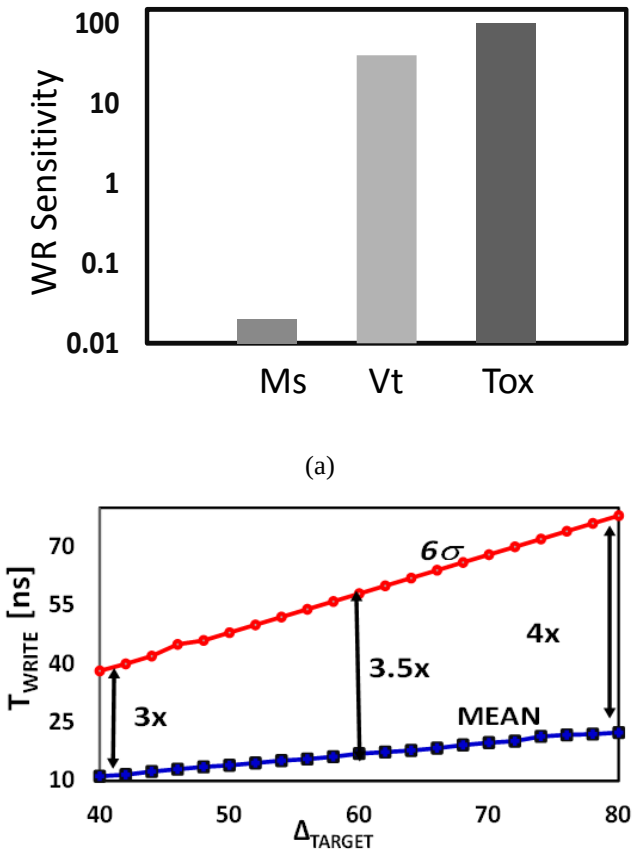

Figure 5: (a) Sensitivity of WR time to different process and material parameters. The three main components have been shown here. The nominal WR time of the MTJ cell is 10ns (Δ=40). (b) The WR time of a mean cell and a 6σ cell with varying Δ showing the large increase in WR time between the nominal and 6σ corners.

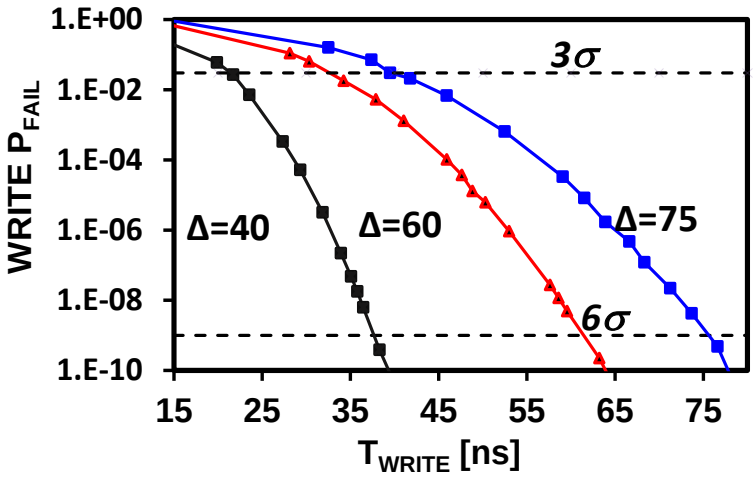

Figure 6: Write failure probability

Figure 6 shows WR P_{FAIL} as a function of Δ. It can be noted that higher temperature leads to a greater variability in WR time and increases the 6σ margin.

4.2 Read Operation & Failure

Similar analysis of RD has been performed as WR. Sensitivity of RD for a parameter p is defined as $S= (\partial T_{RD}/T_{RD})/ (\partial p/p)$. The sensitivity for RD has been found to have a large dependence on the transistor threshold voltage V_{TH}, the MgO thickness T_{OX} and the TMR of the MTJ as seen in Figure 7(a). The reliability of the Read operation is correlated with the difference in the perceived on and off resistances of the cell. These three process parameters have the maximum effect on the read time and extreme variations (>6σ) in them lead to read failures in STT-RAM bit-cells.

RD Fault Models because of parametric variation: The RD is characterized by two failure modes depending on the origin of the failure mode:

(1) **Incorrect Read Fault (IRF):** The inability of the cell to distinguish between a '0' and '1' due to low READ current and/or low TMR (figure 7(b)). The degree of impact of each parameter is again in tune to the parameter sensitivity identified earlier (figure 7(a)).

(2) **Read Disturb Faults (RDF)**: The read current for a cell is so high that the value in the cell flips during RD (fig 7(b)). A lower transistor V_{TH} or lower MTJ resistance can lead to higher than nominal RD current. This can cause an inadvertent bit flip causing RDF. This is further aggravated in a weak cell whose stored internal energy (Δ) is less than a nominal target of 60. In the current study, we consider RDF in only one direction, namely a bit flip occurring when reading a stored value of 1. In figure 7(b) IRF is shown at 25^{O}C and 100^{O}C. Since IRF is thermal noise induced, its probability decreases with decreasing temperature and the 6σ margin needs to be characterized for the highest expected operating temperature.

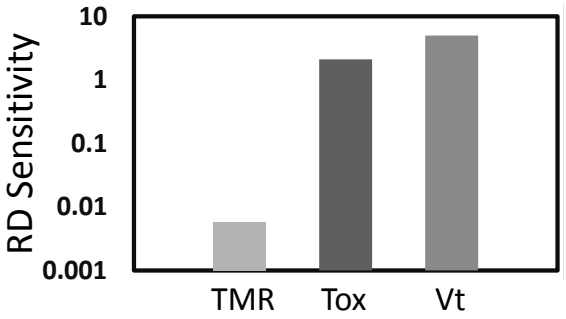

(a)

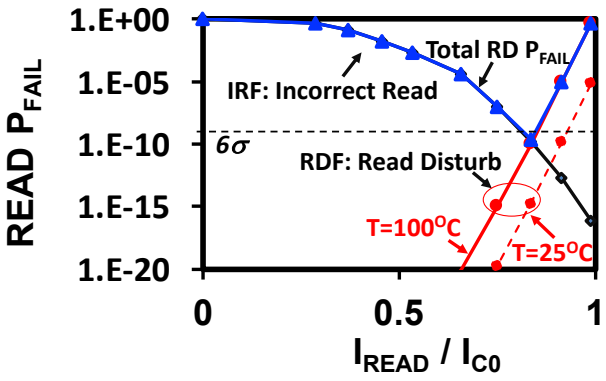

(b)

Figure 7: (a) Sensitivity of RD time with process and material parameters. (b) RD failure probability as a function of read current. RDF is simulated at 100^{O}C. RDF increases with higher temperature. IRF is calculated at 100^{O}C.

4.3. Data Retention & Failure

Finally, a bit-cell can lose its state due to thermal noise, a problem more prominent in scaled bit-cells with decreasing Δ. Such a fault primitive is called **Retention Fault (RTF)**. Figure 8 shows the average retention time in a nominal and a 6σ cell for varying Δ_{TARGET}, (which has been characterized at 25^{O}C). For 7yr retention for a 6σ cell, Δ_{TARGET} ~60 is required. A comparison of figure 5(b) and figure 8 also reveals the fundamental trade-off between writability and retention. We also note a large σ/μ showing long tails in the failure probability and this is aggravated at elevated temperatures. The key fault models and parametric variations leading to these faults are summarized in Table 2.

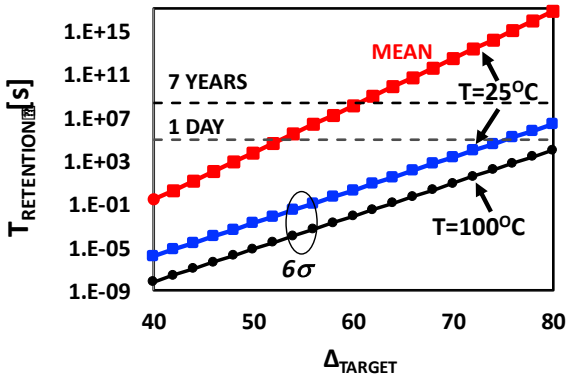

Figure 8: Average retention time vs target Δ

TABLE 2 : Faults due to extreme parametric variations

Fault Model	**Affects**	**Key Cause**
Transition Fault (TF)	WR	WR Time > 6σ of nominal
Incorrect Read Fault (IRF)	RD	Low TMR, low READ current
Read Disturb Fault (RDF)	RD	High RD current due to low transistor V_t, causes bit-flip
Retention Fault (RTF)	Retention	$\Delta < \Delta_{TARGET}$ with guard-band

CHAPTER 5

DEFECTS AND FAULT MODELS

In the previous chapter, we have seen the role of extreme variations in different failure modes for STT-RAM. In particular, we have seen how material, device parameters and thermal effects can cause design parameters to exceed 6σ targets and cause faults in high volume manufacturing (Table 2). Apart from variations, defects in the arrays are also principal sources of failures. In this chapter, we will consider all the possible defects inside a bit-cell and between bit-cells and their fault manifestations. Defects in a hybrid CMOS memory cell can manifest in the form of opens and shorts between various terminals [14]. Even if a cell is designed and laid out according to the design rules, there is a non-zero probability that some defects might appear during High Volume Manufacturing. [30] points out that the high resistance defects (opens) are typically caused due to salicidation, incompletely filled vias or electromigration in interconnects. Similarly, resistive shorts are also caused due to variability in the manufacturing process. In case of STT-MRAM, these defects may form during the transistor fabrication or at BEOL MTJ integration process. Authors in [12] and [13] have analyzed the various defects in SRAM array. In [13] the authors have identified static and dynamic fault models in SRAM. Similarly in [12], 18 potential defects locations in SRAM arrays have been shown. Similar defect injection and analysis methodologies have been suggested in [14] for Memristor arrays. Authors in [14] developed on this framework and provided a study of defects injected at various locations in a Memristor array identifying only the static faults. However in resistive memories such as Memristor arrays or STT-MRAM, bridge defects might occur between adjacent cells that can cause dynamic faults when two or more cells switch simultaneously. In this analysis, we focus on static faults as well as dynamic faults.

To comprehensively study all the defect models, we first categorize them as intra-cell (within a cell) and inter-cell (cell-to-cell) defects and then study their manifestation as

faults. We have identified a total of 25 fault locations for injecting electrical faults for the analysis. The resistive shorts between two nodes (*node1* and *node2*) are denoted by $RS_{<node1- node2>}$. The high resistance opens at *node* are denoted as $RO_{<node>}$. In addition to the Write faults listed in Table 2, defects manifest traditional fault models [13]:

(a) Stuck At Fault (SF0 or SAF1): Here resistive bridges short WL or node T0 (between transistor and MTJ) to either

VDD (SF1) or GND (SF0).

(b) Coupling Fault (CF): Here the process of WR on a neighboring cell can disturb the value in the victim. More details on the defects that can cause CF will be discussed next.

The fault models excited by defects and their key causes are summarized in Table 3. We consider that Retention Failure (RTF) is not induced by resistive defects.

5.1. Intra-Cell Defects and Faults Models:

The four terminals of the cell (BL, SL, WL and T0, the internal node) are considered and defects and bridges are injected covering all the nodes as shown in figure 9 (a)-(c). The opens and shorts are modeled as resistors (open: 1kohm to 1Meg ohm and short: 10 ohm to 10kohm). It is observed that the identified intra-cell opens lead to faults in both 1 to 0 and 0 to 1 transitions by impeding the write current. A short explanation of each defect

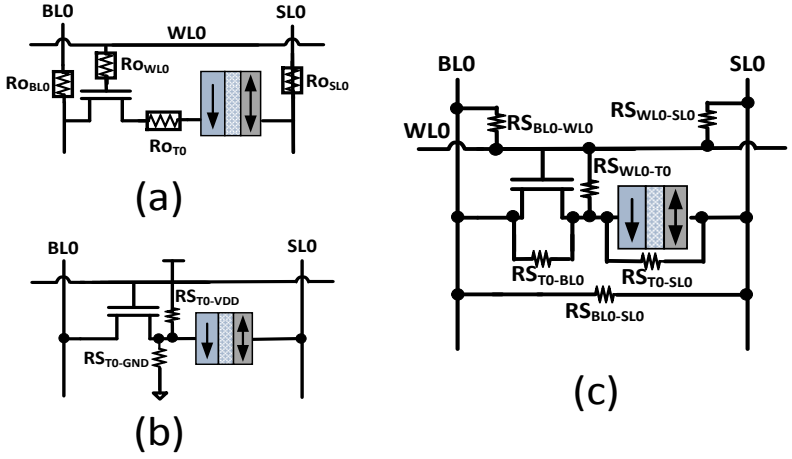

Figure 9: Intra-cell Defects: (a) Opens (b) Stuck at rails (V_{DD} and GND), and (c)

type and its fault manifestation is given below. The information is also succinctly summarized in Table 4.

Intra-cell opens:

1. **RO_{BL0}**: Degraded BL voltage leads to lower drive in 1 to 0 transitions and vice versa and leads to Transition Fault (TF). It also causes Incorrect Read Fault when a 0 is read because of insufficient BL discharge.
2. **RO_{WL0}**: A weak turn on of the access transistor, affects the write current causing TF. It also causes Incorrect Read Fault when a 0 is read because of insufficient BL discharge due to lower read current.
3. **RO_{SL0}:** Similar to RO_{BL0}.
4. **RO_{T0}**: This adds series resistance to the MTJ stack, resulting in lowering of write currents, causes TF. Due to low read currents, lesser BL discharge in the read time leads to IRF for Read 0 operation. It is equivalent to a SF1 as the bit-cell is always read as 1.

TABLE 3: Defect induced Faults

Fault Model	**Affects**	**Key Cause**
Transition Fault (TF)	WR	Relative Weak WR current due to stray resistive paths
Coupling Fault(CF)	WR	Neighboring cells switching
Stuck At Fault(SF)	WR	T0 , WL stuck at VDD or GND
Incorrect Read Fault (IRF)	RD	Current miscorrelation due to defects affecting WL,BL
Read Disturb Fault (RDF)	RD	Electrical disturbance at T0 node due to larger than normal RD current

Intra-cell shorts:

1. **$RS_{T0\text{-}BL0}$**: This leads to read faults (both IRF and RDF) as the WL now does not play any role in controlling the RD current through the bit-cell.

2. **$RS_{T0\text{-}SL0}$**: Here, TF are caused in both directions because of a lower resistance path parallel to the MTJ. This shunts the WR current from the MTJ causing slower transitions or no transitions at all.

3. **$RS_{BL0\text{-}WL0}$**: This affects transitions from 0 to 1 since WL0, which is pulled high, has a path to ground through BL0. This leads to TF. This also causes RDF because of increased WL drive.

4. **$RS_{WL0\text{-}T0}$**: This affects transitions from 1 to 0 because of compromised WL drive and causes TF. Because of the inability of the WL to control the RD current, RDF is also increased.

Table 4: Defect & Fault Models with intra-cell defects

Defect Type	Location	Write Fault model	Write Data Pattern (Victim)	Read Fault model	Read Data Pattern (Victim)
Open	BL0	TF0,TF1	xWx	IRF0	R0
	WL0	TF0,TF1	xWx	IRF0	R0
	SL0	TF0,TF1	xWx	IRF0	R0
	T0	TF0,TF1	xWx	IRF0	R0
Shorts	BL0 - T0		xWx	IRF1,IRF0, RDF	R1
	T0 - SL0	TF0,TF1	xWx	IRF1	R1
	WL0- BL0	TF0	xW1	RDF	R0
	WL0-T0	TF0	xW0	RDF	R0
	WL0-SL0	TF0	xW0	IRF1	R1
	BL0-SL0	TF0	xW0	IRF1	R1
	T0-VCC	SF0	xWx	IRF0	R0
	T0-GND	SF1	xWx	IRF1	R1

5. **$RS_{WL0\text{-}SL0}$**: This causes TF from 1 to 0 because the WL drive is weakened due of path to ground through SL0. Causes IRF1 due to slow BL discharge.

6. **$RS_{BL0\text{-}SL0}$**: Here a short affects transition from 1 to 0 causing TF. The BL drive is weakened due to path to ground through SL0. This also leads to IRF1 due to slow BL discharge.

7. **$RS_{T0\text{-}VCC}$**: Cell stuck at 0: Here 0 to 1 transition not possible because of zero potential difference across MTJ. The cell is always read as 0.

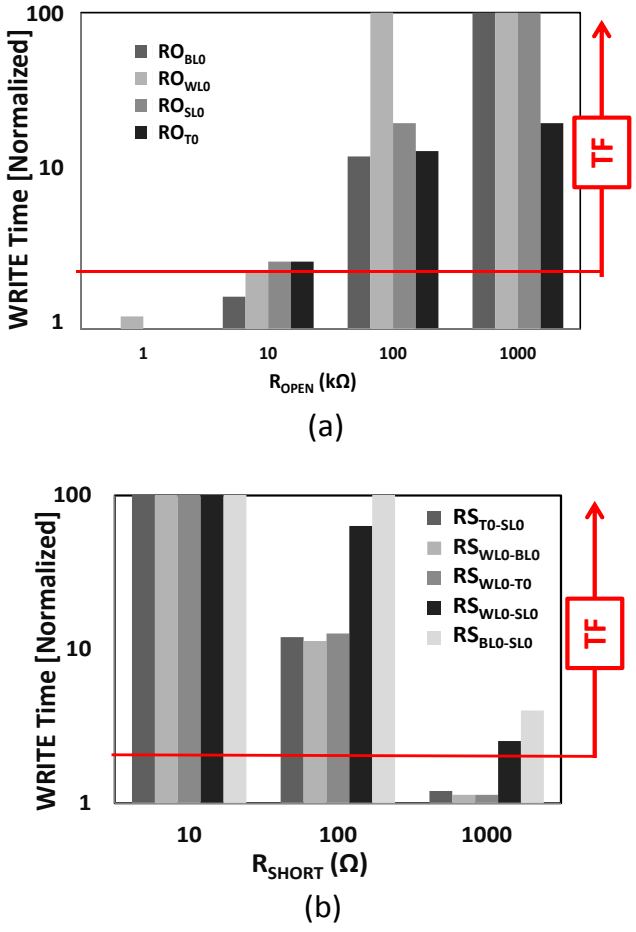

Figure 10: Role of resistive defects on WR time: (a) role of resistive opens from figure 9(a) on WR time and (b)role of resistive shorts from figure 9(c) on WR time. The horizontal line shows the 6σ margin, above we see WR Transition Faults (TF).

8. **$RS_{T0\text{-}GND}$**: Cell stuck at 1: Here 1 to 0 transitions not possible because of zero potential difference across MTJ. The cell is always read as 1. These defects and the WR and RD fault models they excite are shown in Table 3. Here, *x*W*y* refers to a cell whose original value is *x* and we are trying to write *y*. R*x* refers to reading a value of *x* from a cell. $x, y \in \{0,1\}$. xW0/xW1 refers to writing 0/1 independent of the stored value. xWx refers to any WR process on the cell.

Key Observations: For intra-cell opens, any WL open defect sensitizes the TF even for relatively small values of the defect resistance (figure 10). Correspondingly any short at node T0 causes TF or SAF (if the short is to V_{DD}/GND). On the other hand, shorts across the MTJ decreases RD margin (activates IRF) and across the transistor increases the RD current (causes RDF). Figure 11 illustrates their corresponding sensitivities. Intra-cell opens increase the RD time by decreasing the RD current and cause IRF as shown in figure 11(a). Resistive intra-cell opens lead to IRF where any cell whose RD time is over the 6σ margin (horizontal line) has IRF as shown in figure 11(a).Shorts across the MTJ can cause IRF due to degraded margin whereas shorts across the transistor can cause RDF due to high current. Corresponding P_{FAIL} for RD for different values of short is shown in figure 11(b).

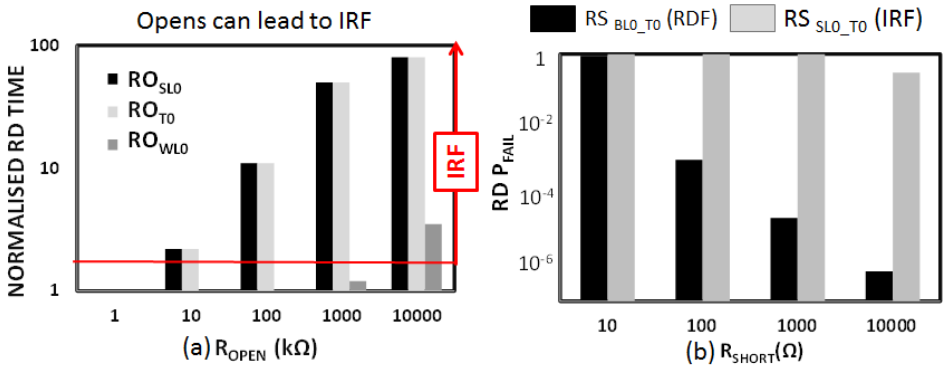

Figure 11: Effect of intra-cell resistive defects on Read (a) effect of resistive opens on RD (b) P_{FAIL} for RD for different values of resistive shorts.

5.2. Inter-Cell Defects and Faults Models:

Inter-cell defects are associated with resistive shorts between the nodes of the victim cell and those of an aggressor cell. To study the defect and fault models, we consider a 2x2 cell array, as shown in figure 12. We observe the presence of 13 possible defects that can affect RD/WR of the cell. We model the faults as resistive shorts and sweep the resistance values

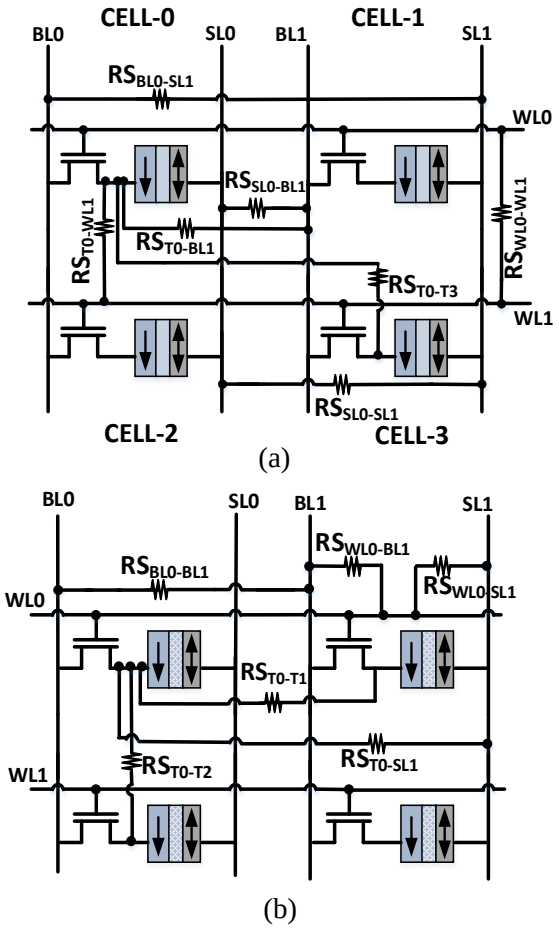

Figure 12: Inter Cell Defects (The defects have been listed in Table 5)

from 10 ohm to 10kohm and the simulation is performed at an array level to observe the effects. The victim cell considered is cell-0 and the aggressors are cells 1, 2 or 3. In the inter-cell defects, apart from static CF's we identify dynamic faults occurring due to data dependent CF's which have not been studied in resistive memories before. These faults get activated when certain pattern is being written into the aggressor and victim cell simultaneously, causing the cell bias voltages to interact with one another and thereby

compromising the drive strengths of each cell. These faults are clearly observable when the analysis is performed at a word level wherein neighborhood cells, when written together, affect each other's writability. The effect of these faults on the victim cell is described below and succinctly captured in Table 5.

Inter-cell shorts:

1. **$RS_{BL0\text{-}SL1}$**: This short causes TF when both cells are written to 0 together because of weakening of BL drive. IRF of state 0 is caused because of weak BL discharge.

2. **$RS_{SL0\text{-}SL1}$**: This cases TF when cell-0 is written 0 and cell-1 is written 1. No effect on Read is noted as both SL0 and SL1 are connected to ground.

3. **$RS_{SL0\text{-}BL1}$**: This leads to TF when cell-0 is written 1 and cell-1 is written 0 because the overall drive of SL0 is weakened.

Table 5: Defect and Fault Models with inter-cell defects

Location	Agressor Cell	Write Fault model	Write Data Pattern (Victim)	Write Data Pattern (Aggressor)	Read Fault model	Read Data Pattern (Victim)
BL0-SL1	1	TF0	xW0	xW0	IRF0	R0
SL0-SL1	1	TF0	xW0	xW1	No effect	NA
BL1-SL0	1	TF1	xW1	xW0	IRF0	R0
T0-WL1	1,2	SA1F,CF	xW0	Idle	IRF0	R0
T0-SL1	1	SA1F	xW0	xW0	IRF1	R1
T0-BL1	1	SA1F	xW0	xW1	IRF1	R1
T0-T1	1	SA1F,CF	xW0	xW1	RDF	R0
T0-T2	2	SA1F,CF	xW0	Idle/xW1	RDF	R0
T0-T3	3	SA1F,CF	xW0	Idle/xW1	IRF1	R1
BL0-BL1	1	TF1	xW1	xW0	IRF1	R1
WL0-BL1	1	SA1F	xW0	xW1	RDF	R0
WL0-SL1	1	SA1F	xW0	xW1	IRF0	R0
WL0-WL1	1,3	CF	xWx	Idle	IRF0	R0

4. **$RS_{T0\text{-}WL1}$**: When WL0 is high and WL1 is low, SAF1 is caused because any drive from BL0 while writing 0 passes to ground through WL1 rather than switching the MTJ. This causes IRF1 because of the fast discharge of BL0.

5. **$RS_{T0\text{-}SL1}$**: This short leads to SA1F when cell-1 is written0 because the current from BL0 has a path to ground through SL1. It causes IRF1 because BL gets discharged faster.

6. **$RS_{T0\text{-}BL1}$:** This excites SA1F when cell-1 is written1 because there is a very low potential difference across the MTJ. It causes IRF1 because BL gets discharged faster.

7. **$RS_{T0\text{-}T1}$**: This causes SA1F when cell-0 is written0 and cell-1 is written 1 because there is a very low potential difference across the MTJ. It also leads to RDF because of coupling from cell-1 to the victim cell.

8. **$RS_{T0\text{-}T2}$**: This leads to SA1F when cell-2 is written1 because there is a very low potential difference across the MTJ. This also leads to RDF because switching in cell-2 couples to cell-0.

9. **$RS_{T0\text{-}T3}$**: It causes SA1F when cell-3 is written 1 because there is a very low potential difference across the victim MTJ. It also leads to IRF1 because BL gets discharged faster.

10. **$RS_{BL0\text{-}BL1}$**: This causes TF when cell-0 is written1 and cell-1 is written 0 because the drive of BL0 is weakened due to short to ground. It also leads to IRF1 because BL0 gets discharged faster.

11. **$RS_{WL0\text{-}BL1}$**: This causes SA1F when cell-0 is written 0 and cell-1 is written 1 because the drive of WL0 is weakened due to short to ground. Further, RDF is increased because of higher WL0 drive during Read.

12. **$RS_{WL0\text{-}SL1}$**: This leads to SA1F when cell-0 is written 0 and cell-1 is written 0 because the drive of WL0 is weakened due to short to ground. It also leads to IRF0 because of lower WL0 drive during Read thus slower BL0 discharge.

13. **$RS_{WL0\text{-}WL1}$**: This leads to CF when cell-0 is written 0 or 1 and cell-1 is idle the drive of WL0 is weakened due to short to ground. It also causes IRF0 because of lower WL0 drive during RD which slows down the BL0 discharge.

Key Observations: It is observed from figure 13 that any short involving the internal node T0 or the WL0 have a large effect on the WR time causing a TF. Defects bridging the BL0 and SL0 with neighboring cell terminals are relatively softer in impact as seen from the figure 13. The critical fault model is the ***data-dependent*** CF. The anti-parallel cell resistance is in the order of ~10kΩ. Hence any short which drains away WR current (even if the short resistance is ~kΩ) causes TF. The node T0 is most sensitive to CF and the probability of CF for T0 bridges is shown. As noted earlier, these arise in hybrid CMOS memory arrays because of the different bias conditions used for writing logic 1 and 0 and this can lead to inadvertent WR. The fault models activated with these sdefects and the data patterns sensitizing these faults are shown in Table 5. For example, when writing 0 to both cell-0 and cell-1, if there is a bridge between BL0 and SL1 (figure 12(a)) this leads to weakening of BL0 possibly leading to a TF0 (transition to 0 fault). Also shorts between T0 and WL1 lead to static coupling faults where, if cell-2 is being read or written (WL1 is

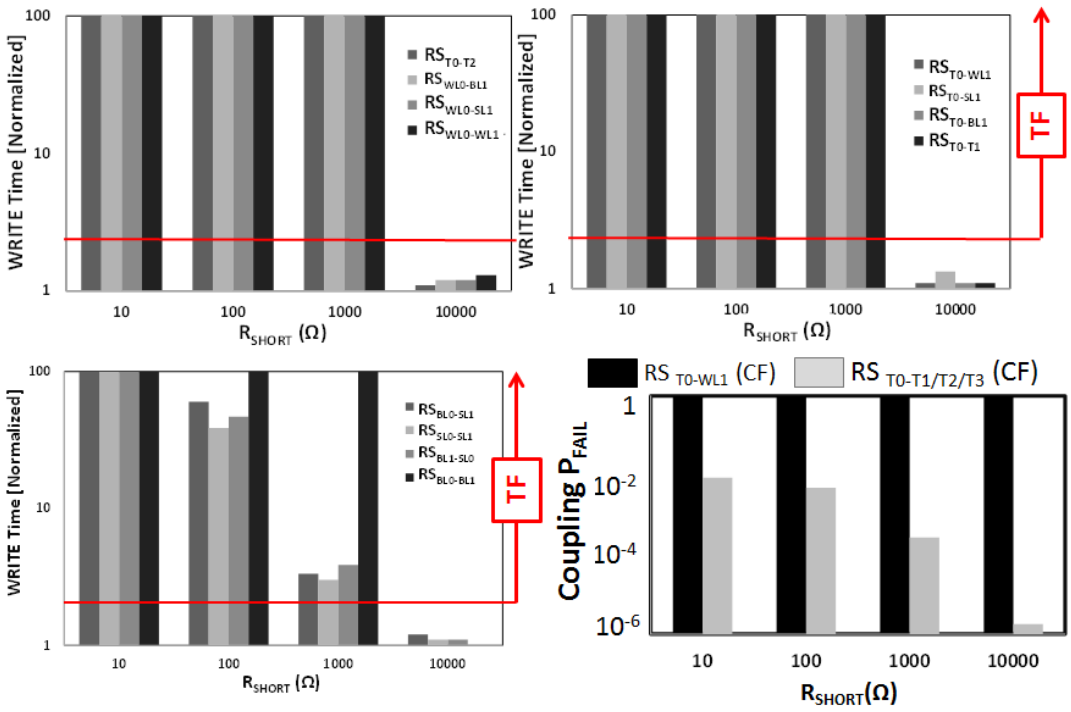

Figure 13: Effect of Inter-cell resistive defects on Write and Read

high), the short drives current through MTJ0 possibly switching its state inadvertently. We note that shorts to the node T0 cause CF; and the data patterns (on neighbors) which sensitize these faults are shown in Table 5. Finally, a short between WL0 and WL1 can also cause both WL being simultaneously turned on (last row of Table 5) causing an inadvertent WR on cell-0. Most of the inter cell defects activate IRFs. Inter cell defects occurring at T0 can potentially lead to RDF when the neighboring cell is being read or written. The short at WL0-BL1 also result in RDF as shown in Table 5. It should be noted that defect analysis presented here captures the effect on nominal cells. In an already weak cell, the defects have more pronounced effects leading to faults. This is shown in figure 14 for representative defects. It can be compared to figures 10 and 11 for a comparative understanding of the role of defects in already weak (3σ) cells.

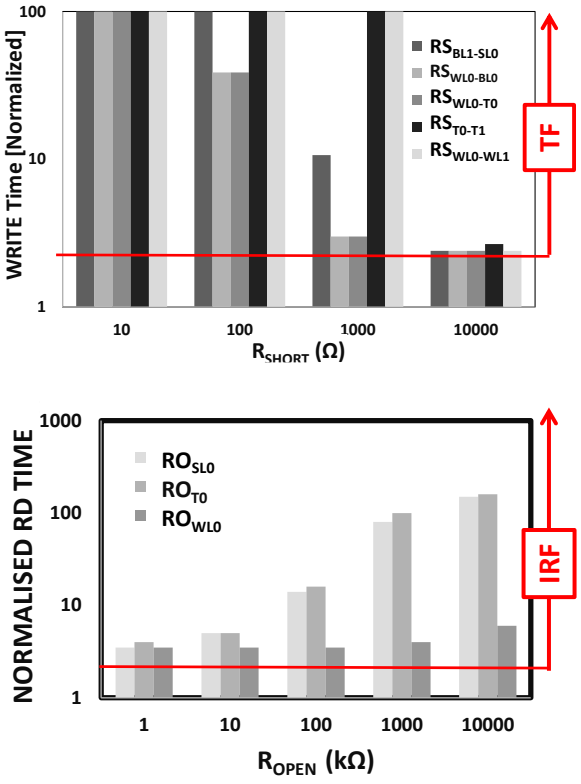

Figure 14: Effect of defects on WR, RD in a (3σ) cell

CHAPTER 6

FAULT EXCITATION

An analysis of defects and corresponding faults leads to the notion of test patterns and test coverage. In this chapter, we compare coverage of the faults described here under existing test conditions. In particular, tests for traditional SRAM arrays and recent work on testing of resistive Memristor arrays are of interest.

Traditional RAM testing uses March tests to detect faults in an array. These have been refined over many generations of technology and, in high volume manufacturing, they can provide very high fault coverage. Several March tests like MATS++, March A, March B, March C- etc. have been proposed for SRAM arrays to detect the SAF, TF, CF fault models [31]. March C- has been shown to have a good coverage for most of these faults. These March tests detect the static SAF, Transition and Coupling Faults in the array [31]. In STT-MRAM, for faults that have been discussed in this work, MARCH C- test can cover most of the SAF, TF and CF. However, this test is not sufficient for detecting dynamic faults that include single cell dynamic Functional Fault Models (FFMs) and Two-cell dynamic FFMs [13]. The authors in [13] have introduced March RAW and March RAW1 to detect dynamic faults for one-cell and two-cell FFMs. March RAW tests will cover dynamic faults described in Table 5.

In [17] the authors have investigated new fault models in resistive arrays with Memristor based bit-cells. An existing March test (March MOM) in the context of Memristor arrays shows good coverage but the authors have noted that dynamic Write disturb fault (dWdf) is not covered by March MOM. Hence they introduced a new March test, namely March 1T-1R which covers dynamic faults in a single-cell in a Memristor. As STT-MRAM does not exhibit incremental write, the dWdf is not seen here. Also the March 1T-1R, although covers static faults and single-cell dynamic faults, the two-cell dynamic faults discussed in chapter IV which involve data dependent coupling when writing two neighboring cells

simultaneously are not covered. Such faults as summarized in Table 5 for inter-cell defects are seen when the patterns given in the table for Aggressor and Victim are written simultaneously, e.g., while writing a word. In essence, these faults are sensitized during Word level writing of the memory and thus require Word Oriented March tests for detection.

For the 2x2 array considered in this work, the word size being 2, the March RAW (Read after Write) [13] is taken and extended to the word size to detect faults given in Table 4 and 5, it can be described as:

{⇑ (w00, r00); ⇑ (w01, r01); ⇓ (w10, r10)}

In this current work, we have only discussed electrical defects and the corresponding faults. Magnetic field based coupling between cells may lead to Neighborhood Pattern Sensitive Faults (NPSF) that are often noted in DRAM. The origin of such faults is briefly described in [6].

CHAPTER 7

CONCLUSIONS AND FUTURE WORK

This work presents a comprehensive analysis of variations and defects in STT-MRAM. Fault models corresponding to the various resistive defects have been discussed. The results and observations will enable test pattern generation for target fault coverage.

The key observations of this work are summarized below:

1. In STT-MRAM, the parameter variations having most sensitivity for Write failure are the transistor threshold voltage, the thickness of the MgO dielectric and the saturation Magnetization of the free layer Ms. Temperature plays a key role in inducing thermal noise and it exacerbates the role of parametric variations.
2. The parameters whose variation has the most effect on Read failure probability are the transistor threshold voltage, the thickness of the MgO dielectric, and the Tunnel Magnetization Ratio.
3. The electrical defects bearing most sensitivity on Write failure probability are those occurring at the internal node T0 and those involving the Word line WL.
4. Shorts across the access transistor can cause Read disturb by flipping the bit-cell, thereby causing failure and this is exacerbated at higher temperature.
5. Shorts involving the internal node T0 can cause Incorrect Read Faults.
6. The failure probability for Read or Write gets worse in the presence of bridge defects in an already weak cell due to parameter variations, pushing errors from the soft error domain to the hard error domain where a relaxed clock frequency will not be able to recover the weak cells.
7. Bridge faults are shown to have profound effects on Write when two cells bridged by a fault are written simultaneously with a certain pattern. These faults are termed in this study as data-dependent Coupling Faults. March tests extended to a word granularity are needed to identify these faults.

The area of defect analysis and fault diagnosis in STT-MRAM is an increasingly important research vector as commercialization of STT-MRAM becomes a reality. The role of magnetic coupling and alternative device structures on defects and fault models will be addressed be interesting areas to be pursued in future. Also, since non-volatility and retention are one of the most attractive features of STT-MRAM, it becomes important to characterize retention properties and build a fast BIST circuitry for retention test of STT-MRAM for both high volume and bench characterization. In spite of its many promises, STT-RAM presents serious challenges in materials, integration, circuits and applications. As academic and industrial researchers investigate the paradigm, several key technological innovations are expected to pave the way for embedded STT-RAM arrays in future SoCs.

REFERENCES

[1] S. A. Wolf, et al. “The promise of nanomagnetics and spintronics for future logic and universal memory,” *Proc. IEEE*, vol. 98, no. 12, pp. 2155–2168, Dec. 2010.

[2] Ki Chul Chun; Hui Zhao; Harms, J.D.; Tae- Hyoung Kim; Jian-Ping Wang; Kim, C.H., "A Scaling Roadmap and Performance Evaluation of In-Plane and Perpendicular MTJ Based STT-MRAMs for High-Density Cache Memory," in *Solid- State Circuits, IEEE Journal of* , vol.48, no.2, pp.598-610, Feb. 2013

[3] K L Wang et al. “Low-power non-volatile spintronic memory: STT-RAM and beyond”, J. Phys. D: Appl. Phys**.**,vol 46, no. 7, Feb. 2013.

[4] Kim, J.P et al. "A 45nm 1Mb embedded STT-MRAM with design techniques to minimize read-disturbance," *VLSI Circuits (VLSIC), 2011 Symposium on*, vol., no., pp.296,297, 15-17 June 2011.

[5] Noguchi, H et al. "A 3.3ns-access-time 71.2μW/MHz 1Mb embedded STT-MRAM using physically eliminated read-disturb scheme and normally-off memory architecture," *Solid- State Circuits Conference - (ISSCC), 2015 IEEE International* , vol., no., pp.1,3, 22-26 Feb. 2015

[6] A. Raychowdhury, D. Somasekhar, T. Karnik, and V. De, “Design space and scalability exploration of 1T-1STT MTJ memory arrays in the presence of variability and disturbances,” in *Proc. IEEE IEDM*,Dec. 2009, pp. 1–4.

[7] Jing Li; Augustine, C.; Salahuddin, Sayeef; Roy, K., "Modeling of failure probability and statistical design of Spin-Torque Transfer Magnetic Random Access Memory (STT MRAM) array for yield enhancement," *Design Automation Conference, 2008.*

[8] Dorrance, R.; Fengbo Ren; Toriyama, Y.; Hafez, A.A.; Yang, C.-K.K.; Markovic, D., "Scalability and Design- Space Analysis of a 1T-1MTJ Memory Cell for STT-RAMs," in *Electron Devices, IEEE Transactions on* , vol.59, no.4, pp.878-887, April 2012.

[9] Yaojun Zhang; Xiaobin Wang; Yiran Chen, "STT-RAM cell design optimization for persistent and non-persistent error rate reduction: A statistical design view," *Computer-Aided Design (ICCAD), 2011 IEEE/ACM International Conference on* , vol., no., pp.471,477, 7-10 Nov. 2011.

[10] Panagopoulos, G.D.; Augustine, C.; Roy, K., "Physics-Based SPICE-Compatible Compact Model for Simulating Hybrid MTJ/CMOS Circuits," *Electron Devices, IEEE Transactions on* , vol.60, no.9, pp.2808,2814, Sept. 2013.

[11] Fonseca, R.A.; Dilillo, L.; Bosio, A.; Girard, P.; Pravossoudovitch, S.; Virazel, A.; Badereddine, N., "Impact of Resistive-Bridging Defects in SRAM Core-Cell," *Electronic Design, Test and Application, 2010. DELTA '10. Fifth IEEE International Symposium on* , vol., no., pp.265,269, 13-15 Jan. 2010.

[12] Rei-Fu Huang; Yung-Fa Chou; Cheng-Wen Wu, "Defect oriented fault analysis for SRAM," *Test Symposium, 2003. ATS 2003. 12th Asian* , vol., no., pp.256,261, 16-19 Nov. 2003.

[13] Hamdioui, S.; Al-Ars, Z.; van de Goor, A.J., "Testing static and dynamic faults in random access memories," *VLSI Test Symposium, 2002. (VTS 2002). Proceedings 20th IEEE* , vol., no., pp.395,400, 2002.

[14] N. Z. Haron and S. Hamdioui, "On defect-oriented testing for hybrid CMOS/Memristor memory," in IEEE Asian Test Symp. (ATS), Nov. 2011.

[15] Kannan, S.; Karimi, N.; Karri, R.; Sinanoglu, O., "Detection, diagnosis, and repair of faults in memristor-based memories," in *VLSI Test Symposium (VTS), 2014 IEEE 32nd* , vol., no., pp.1-6, 13-17 April 2014.

[16] Hamdioui, S.; Taouil, M.; Haron, N.Z., "Testing Open Defects in Memristor-Based Memories," in *Computers, IEEE Transactions on* , vol.64, no.1, pp.247-259, Jan. 2015

[17] Chen, Yong-Xiao; Li, Jin-Fu, "Fault modeling and testing of 1T1R Memristor memories," *VLSI Test Symposium (VTS), 2015 IEEE 33rd* , vol., no., pp.1,6, 27-29 April 2015.

[18] O. Ginez, J. Portal, and C. Muller, "Design and test challenges in resistive switching RAM (ReRAM): An electrical model for defect injections," in IEEE European Test Symp. (ETS), May 2009, pp. 61–66.

[19] A V Khvalkovskiy *et al* 2013 *J. Phys. D: Appl. Phys.* **46** 139601

[20] Jing Li; Ndai, P.; Goel, A.; Salahuddin, Sayeef; Roy, K., "Design Paradigm for Robust Spin-Torque Transfer Magnetic RAM (STT MRAM) From Circuit/Architecture Perspective," *Very Large Scale Integration (VLSI) Systems, IEEE Transactions on* , vol.18, no.12, pp.1710,1723, Dec. 2010

[21] Kangho Lee; Kang, S.H., "Design Consideration of Magnetic Tunnel Junctions for Reliable High-Temperature Operation of STT-MRAM," *Magnetics, IEEE Transactions on*, vol.46, no.6, pp.1537,1540, June 2010.

[22] J.Z. Sun, "Spin-current interaction with a monodomain magnetic body:A model study," *Phys. Rev. B*, vol. 62, no. 1, pp. 570–578, Jul. 2000.

[23] Augustine, C et al. "Numerical analysis of typical STT- MTJ stacks for 1T-1R memory arrays," *Electron Devices Meeting (IEDM), 2010 IEEE International*, vol., no., pp.22.7.1,22.7.4, 6-8Dec.2010.

[24] Guenole Jan, et al. "Demonstration of fully functional 8Mb perpendicular STT-MRAM chips with sub-5ns writing for non-volatile embedded memories," in *VLSI Technology (VLSI-Technology): Digest of Technical Papers, 2014 Symposium on* , vol., no., pp.1-2, 9-12 June 2014.

[25] Ikegami, K et al., "Low power and high density STT-MRAM for embedded cache memory using advanced perpendicular MTJ integrations and asymmetric compensation techniques," in *Electron Devices Meeting (IEDM), 2014 IEEE International* , vol., no., pp.28.1.1-28.1.4, 15-17 Dec. 2014.

[26] Ikeda, S et al. "A perpendicular-anisotropy CoFeB–MgO magnetic tunnel junction", Nat Mater, 2010/09/ VL - 9.

[27] Park, J.G et al."Challenging issues for terra-bit-level perpendicular STT-MRAM," in *Electron Devices Meeting (IEDM), 2014 IEEE International* , vol., no., pp.19.2.1-19.2.4, 15-17 Dec. 2014.

[28] Intel Technology Journal. Volume 17, Issue 1, 2013.

[29] Predictive Technology Model: http://ptm.asu.edu/latest.html

[30] Kruseman, B.; Majhi, A.; Hora, C.; Eichenberger, S.; Meirlevede, J., "Systematic defects in deep sub-micron technologies," *Test Conference, 2004. Proceedings. ITC 2004. International*, vol., no., pp.290,299, 26-28 Oct. 2004.

[31] Van de Goor, A.J., "Using march tests to test SRAMs," in *Design & Test of Computers, IEEE* , vol.10, no.1, pp.8-14, March 1993.